High-quality spray-deposited fluorine-doped tin oxide: effect of film thickness on structural, morphological, electrical, and optical properties

Hassan Zare Asl[1] · Seyed Mohammad Rozati[2]

Abstract

High-quality fluorine-doped tin oxide (FTO) thin films were deposited using a low-cost homemade spray pyrolysis apparatus and the effect of film thickness on structural, morphological, electrical, and optical properties were investigated. As the thickness increases, the carrier concentration remains almost unchanged ($\sim 2.6 \times 10^{20}$ cm^{-3}). However, as a result of grain size increase, mobility enhanced considerably (from 19.1 to 40.1 cm^2 V^{-1} s^{-1}), which can be a convincing explanation for resistivity reduction (from 12.0×10^{-4} Ω cm to 6.00×10^{-4} Ω cm). As expected, the FTO thin films were highly transparent in the visible region and naturally decreased by increasing the thickness. The band-gap value of the spray-deposited FTO thin films was estimated, with results showing a gradual reduction with increasing thickness. The figure of merit was calculated for the prepared FTO thin film and an outstanding value of 9.77×10^{-3} Ω^{-1} corresponding to an average transmittance of 78.60 (400–900 nm) and sheet resistance of 9.21 Ω/sq was achieved.

1 Introduction

Due to the extensive variety of applications in electronic and optoelectronic devices as well as the feasibly of deposition using a wide range of methods, transparent conductive oxides (TCOs) have been the center of attention during the last decades. The most practical and well-known TCOs are mainly based on zinc oxide (ZnO), tin oxide (SnO$_2$), and indium oxide (In$_2$O$_3$). A variety of metal dopants have been employed by researchers to modify both the transparency and conductivity of the aforementioned metal oxides, giving rise to promising TCOs such as indium-doped ZnO (IZO) [1], aluminum-doped ZnO (AZO) [2], tin-doped In$_2$O$_3$ (ITO) [3], and antimony-doped SnO$_2$ (SnO$_2$:Sb) [4]. However, it seems that the substitution of primary metal with metal dopant can cause a considerable perturbation on the conduction band, confining the free-carrier mobility and, therefore, conductivity. On the contrary, in the cases of non-metal dopant TCOs such as fluorine-doped SnO$_2$ (FTO) and

fluorine-doped ZnO (FZO), the electronic perturbation is restricted to the valence band, leading to a superior mobility and conductivity [5]. Furthermore, compared to other common TCOs, FTO has almost the least toxicity, lowest cost of production, best mechanical and chemical durability, and best thermal stability [5], the latter making the FTO thin films a wise choice for heat treatment and multilayer deposition [6].

FTO thin films have been deposited via almost all conventional physical and chemical deposition techniques such as sol–gel [7], sputtering [8], pulsed laser deposition [9], chemical vapor deposition [10], and spray pyrolysis [11]. Among the aforementioned methods, the low cost of deposition and suitability for mass production [12] are the main reasons for the extensive application of spray pyrolysis for FTO thin-film deposition.

Clearly, variation of spray parameters has a decisive impact on the characteristics of resulting FTO thin films. Accordingly, there have been numerous studies in which the effect of spray parameters such as temperature [13], solution concentration [14], solution properties [15], and annealing [16] has been investigated.

In the present study, the effect of spray solution volume on the structural, morphological, optical, and electrical properties of FTO thin films has been examined. Varying the

✉ Hassan Zare Asl
  Zare@bkatu.ac.ire

1 Department of Physics, Behbahan Khatam Alanbia University of Technology, Behbahan, Iran

2 Department of Physics, University of Guilan, Rasht, Iran

solution volume primarily leads to FTO thin films with a different thickness and, therefore, different characteristics.

2 Materials and methods

FTO thin films were deposited onto well-cleaned soda lime glass via a homemade spray pyrolysis apparatus endowed with a custom spraying gun. To prepare the 80 ml precursor solution, 5.162 gr of tin chloride dihydrate ($SnCl_2.2H_2O$) was added to 2 ml hydrochloric acid (HCl) (37%) and stirred vigorously for half an hour. As a result, the $SnCl_2.2H_2O$ was dissolved in HCl and a transparent solution was prepared. It is well known that the presence of HCl can break down the strong ionic bonds in $SnCl_2$ and facilitate the pyrolysis reaction and growth of the tin oxide layer on the substrate. More accurately, the reaction between HCl and $SnCl_2$ leads to the formation of $HSnCl_3$ which is an unstable molecule and decomposes during the spray process [17]. Smith et al. [18] investigated the influence of HCl concentration (from 0.03 to 0.7 M) on the starting solution containing $SnCl_2.2H_2O$ and reported that the conversion of $SnCl_2.2H_2O$ into $HSnCl_3$ is maximum for 0.2 M of HCl concentration. As the concentration of HCl exceeds 0.2 M, the possibility of formation of acid molecule $HSnCl_4^-$ and $H_2SnCl_3^+$ increases as well. These molecules are less capable to react at the film surface. In this study, the concentration of HCl (0.3 M) is fairly close to the optimum concentration for the $SnCl_2.H_2O$ conversion.

The resulting solution was diluted by adding 58 ml of deionized water. 0.254 gr ammonium fluoride was utilized as a fluorine source and dissolved in the previously mentioned solution. Finally, 20 ml methanol was added to the solution. To investigate the effect of FTO film thickness, 6, 10, 14, 18, and 22 ml of the resulting solution was spray-deposited on the glass substrate and named T1, T2, T3, T4, and T5, respectively (Table 1). The optimized experimental parameters for spray deposition were the substrate temperature of 500 ℃, nozzle-substrate distance of 287 mm, and carrier gas pressure of 0.9 bar.

The XRD patterns of the deposited FTO thin films were recorded via an X'Pert PRO PANalytical diffractometer with Cu-Kα radiation and 0.026 scan steps. Moreover, an MIRA3TESCAN-XMU field-emission scanning electron microscope (FESEM) was employed to study the surface morphology, measure the thickness, and record the energy dispersive X-ray spectroscopy (EDX) of the FTO thin films. The electrical properties of as-prepared thin films, including carrier mobility, carrier concentration, and resistivity of the resulting films, were monitored via Van der Pauw and Hall effect techniques (Phys Tech) at room temperature. Finally, the optical transmittance and reflectance of the deposited FTO thin films were obtained by a Perkin-Elmer Lambda 25 spectrophotometer.
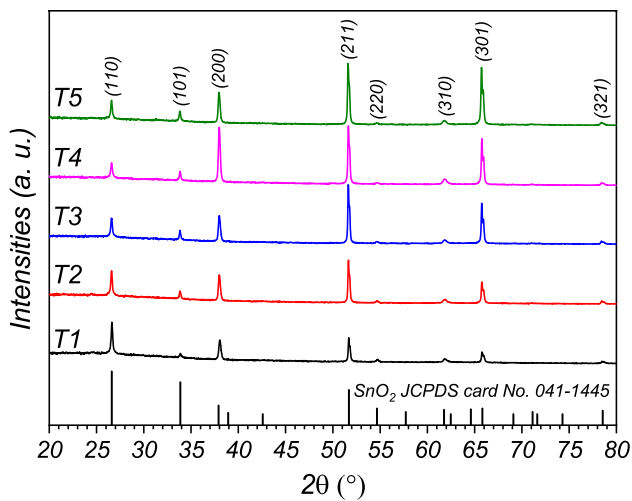
3 Results

3.1 Structural properties

The recorded XRD patterns of the spray-deposited FTO thin films with different thicknesses are presented in Fig. 1. It is evident that there are eight distinctive peaks related to the (110) (101) (200) (211) (220) (310) (301), and (321) planes of the tetragonal SnO_2 structure which are in good agreement with JCPDS card No. 041–1445 [19, 20]. For the T1 sample, the (110) (200), and (211) have the highest intensities, indicating that the mentioned orientations are the dominant orientations. As the thickness increases from T1 to T5, FTO thin films grow mainly with the (211) and (301) orientations to the extent that (211) and (301) orientations have the highest intensities for the T5 samples.

To gain a better understanding of the variation of peak intensities, the texture coefficient (TC) was calculated for prominent peaks [21], and the results are presented in Table 1 and Fig. 2a. As shown in Fig. 2a, the thickness of FTO thin films increases, and the *TC(301)* starts to generally grow drastically from 0.702 for the T1 sample to 4.244 for the T5 sample. Furthermore, the lattice constant *(a, c)* and volume cell *(V)* of the tetragonal FTO thin films were calculated using the

Table 1 The precursor volume, thickness, texture coefficient, and lattice parameters of the spray-deposited FTO thin films with different thicknesses

Sample name	Precursor volume (ml)	Thickness t (nm)	Texture coefficient				Lattice parameter		
			110	200	211	301	a (Å)	c (Å)	V (Å^3)
T1	6	390	0.797	2.364	1.077	0.702	4.7303 ± 0.0003	3.1884 ± 0.0008	71.34
T2	10	570	0.433	2.108	1.289	2.608	4.7377 ± 0.0004	3.1915 ± 0.0004	71.64
T3	14	730	0.241	1.578	1.341	3.736	4.7370 ± 0.0004	3.1924 ± 0.0005	71.63
T4	18	865	0.149	2.607	1.023	3.282	4.7369 ± 0.0003	3.1915 ± 0.0004	71.61
T5	22	965	0.192	1.504	1.125	4.244	4.7381 ± 0.0003	3.1936 ± 0.0003	71.7

Fig. 1 The XRD pattern of the FTO thin films with different thicknesses along with (hkl) planes

lattice spacing (d_{hkl}) of (110) and (101) planes and the following equation [22]:

$$\frac{1}{d_{hkl}^2} = \frac{h^2 + k^2}{a^2} + \frac{l^2}{c^2}. \tag{1}$$

The results are represented in Table 1. For a better understanding of structural characteristics, the Williamson–Hall method was employed to estimate the crystallite size (D) and strain (ε) of the FTO thin films:

$$\beta \cos\theta = \frac{k\lambda}{D} + 4\varepsilon \sin\theta, \tag{2}$$

where θ is the Bragg angle, β is the full width at half maximum, λ is the X-ray wavelength (1.5406Å), and k is a constant (0.9) [23]. The estimated values of the aforementioned parameters are listed in Table 2 and illustrated in Fig. 2b. It is found that both crystallite size and strain increase with increasing thickness, whereas the rate of the increase gradually reduces with thickness to the extent that there is no considerable difference between T4 and T5 crystallite size and strain.

3.2 Morphological properties

The systematic variation in the surface morphology and the cross-section image of the T1, T3, and T5 samples are demonstrated in Fig. 3. Based on FESEM images, the surface morphology of all samples is quite compact and crack-free with rather distinguishable boundaries, while grain size and homogeneity are highly dependent on the thickness of the deposited FTO thin films. The smallest grains belong to the T1 sample in comparison with T3 and T5 samples. Furthermore, the grain size distribution is fairly wide in the former sample. As the thickness

Table 2 The estimated crystallite size, strain, bandgap, and Urbach energy for the spray-deposited FTO thin films with different thicknesses

Sample name	Crystallite size D (nm)	strain $\varepsilon \times 10^{-3}$	Bandgap E_g (eV)	Urbach energy E_U (eV)
T1	89	1.50	3.894	0.133
T2	105	1.56	3.878	0.184
T3	107	1.67	3.872	0.203
T4	112	1.71	3.854	0.254
T5	113	1.72	3.845	0.280
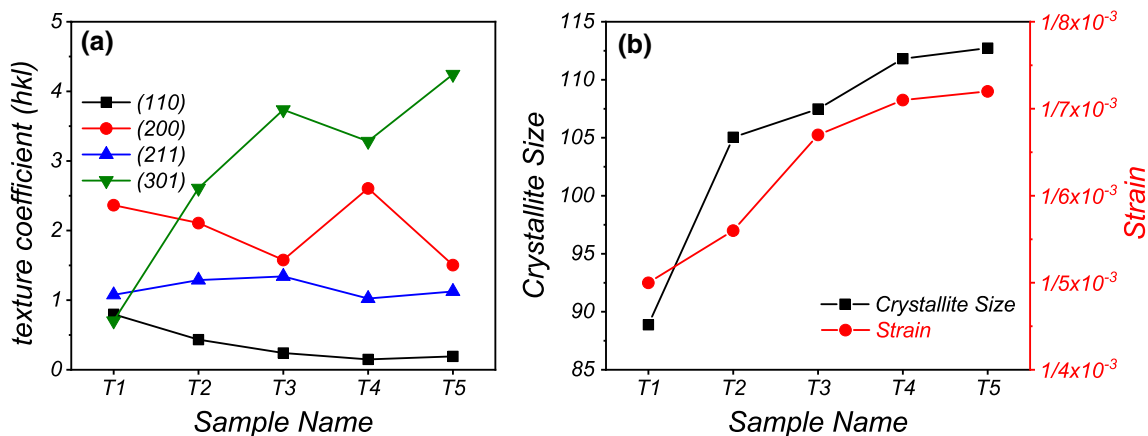
Fig. 2 The variation of **a** (110) (200) (211), and (301) texture coefficients, and **b** crystallite size and strain with thickness for the spray-deposited FTO thin films
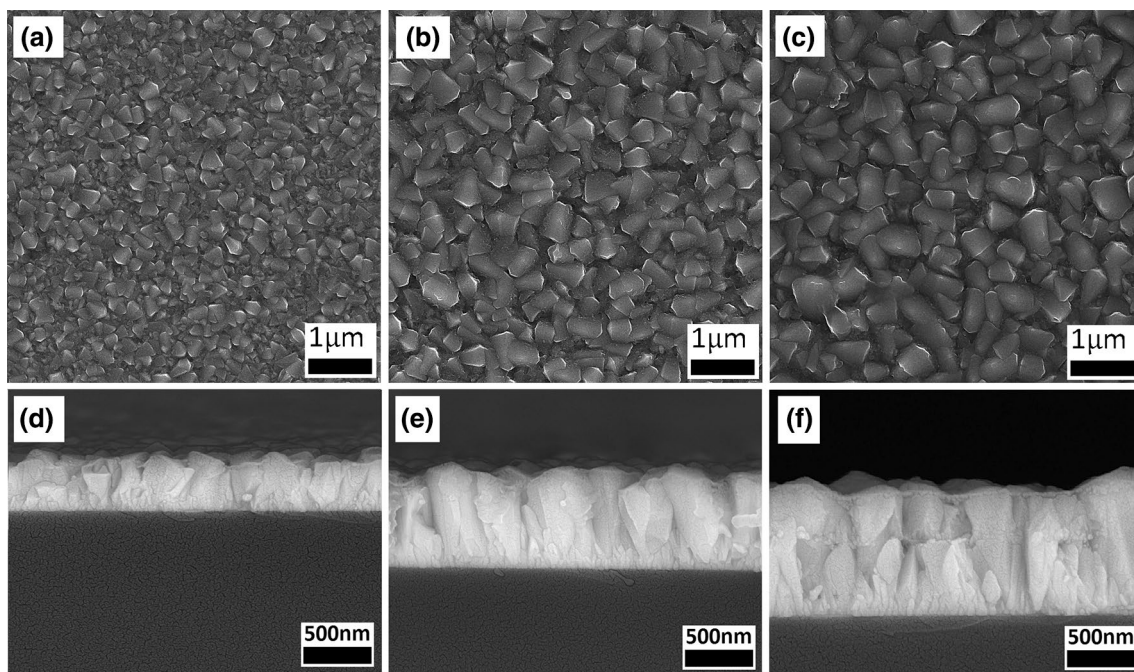
Fig. 3 The surface FESEM and cross-section image of **a**, **d** T1 **b**, **e** T3 **c**, **f** T5 samples

increases, a significant enlargement in grain size as well as a more homogenous size distribution can be observed for T3 and T5 samples which are in good agreement with the XRD results [24]. As discussed in the previous section, as the thickness increases, the FTO thin films grow mainly with the (211) and (301) orientations, which can be a proper explanation for the grain size increase and homogeneity improvement with thickness [25]. Moreover, the results of performed EDX analysis (Fig. 4) confirm the existence of tin (Sn), oxygen (O), and fluorine (F) in sample T5.

Fig. 4 The EDX spectrum of the T5 sample
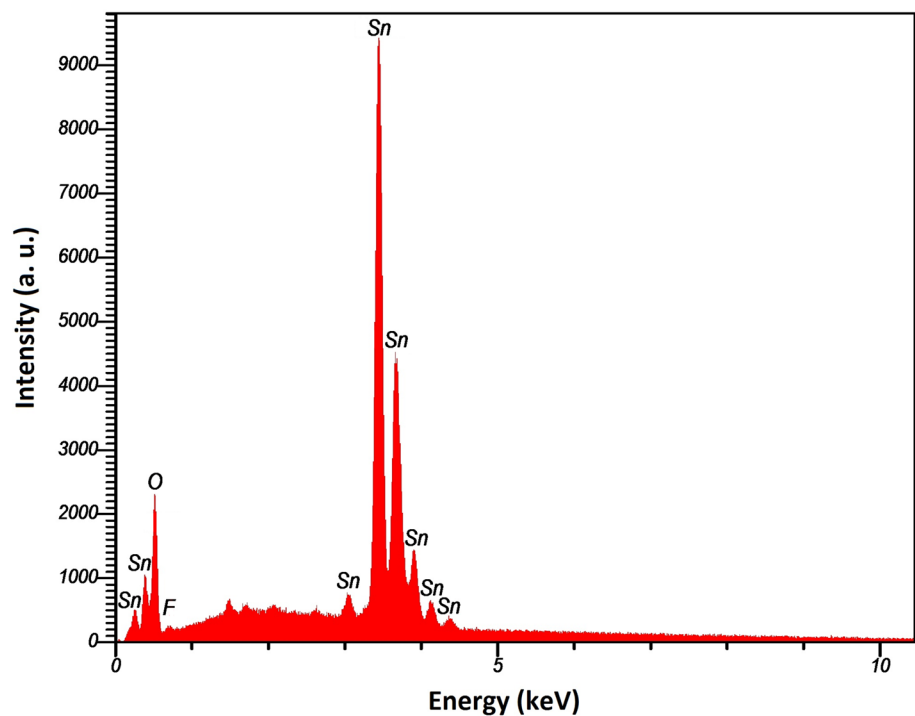
3.3 Electrical properties

To examine electrical characteristics, the Hall effect technique with Van der Pauw configuration was performed on the spray-deposited FTO thin films with different thicknesses, and the results are presented in Table 3. In addition, the variation of resistivity, mobility, and carrier concentration are depicted in Fig. 5. In general, the free-carrier concentration of a semiconductor oxide can be elevated by (i) deviation from stoichiometry, or (ii) introducing an adequate impurity to the main structure. Due to the almost similar radii of O^{2-} (1.40 Å) and F^- (1.36 Å), the substitution of O^{2-} with F^- is quite probable and each substitution gives one free electron to the structure [26]. Accordingly, the considerable value of carrier concentration in the prepared FTO thin films is the direct result of oxygen vacancy and substitution of O^{2-} with F^-. Since all the FTO thin films with different thicknesses were deposited with the same spray condition and F-doping percentage, the carrier concentration remains almost unchanged. On the contrary, by increasing the thickness up to the T4 sample (865 nm), the resistivity of the films improved drastically (from 1.2×10^{-3} Ω cm for T1 to 5.94×10^{-4} Ω cm for T4), and there was no significant change for the T5 sample (6.00×10^{-4} Ω cm). The same enhancement trend can be observed for mobility with increasing thickness, showing that the enlargement of

mobility is responsible for resistivity reduction. The same trend for mobility and carrier concentration variation with thickness has been reported in the literature [27].

Zhang et al. [28] reported that as long as carrier concentration is larger than 5×10^{18} cm^{-3}, lattice vibration scattering dominates the mobility for large crystallite size TCOs at the temperatures more than 100 K. Accordingly, there must be a correlation between the texture variation and the mobility increase in the FTO thin films. As presented in Fig. 6, the variation of the mobility shows remarkable consistency with $TC(301)/TC(110)$ ratio. It has been known that the (110) plane has a high value of atomic density [8, 29]. Furthermore, Korotkov et al. [30] utilized different precursors to deposit SnO_2 thin films with different preferred orientations and showed that the highest value of mobility belongs to the films with (301) preferred orientation. The reduction of the $TC(110)$ and the increase in the $TC(301)$ with increasing thickness and, therefore, reduction in the lattice vibration seem to be the main reasons for the mobility variation [31].

3.4 Optical properties

Figure 7a demonstrates the optical transmittance and reflectance of the spray-deposited FTO thin films with different thicknesses. As a consequence of having the lowest thickness, the highest value of transparency belongs to the T1 sample

Table 3 The electrical characteristics, average transmittance, and calculated figure of merit of the spray-deposited FTO thin films with different thicknesses

Sample name	Mobility m (cm^2 V^{-1} s^{-1})	Carrier concentration n ($\times 10^{20}$ cm^{-3})	Sheet resistance R_{Sh} (Ω/sq)	Resistivity ρ ($\times 10^{-4}$ Ω cm)	Average transmittance (400–900 nm) %	Figure of merit Φ ($\times 10^{-3}$ Ω^{-1})
T1	19.4	2.66	30.9	12.0	87.33	8.35
T2	28.2	2.69	14.4	8.21	79.82	7.29
T3	34.2	2.72	9.21	6.72	78.60	9.77
T4	39.9	2.64	6.87	5.94	70.11	4.18
T5	40.1	2.60	6.22	6.00	67.35	3.09

Fig. 5 The variation of the resistivity, mobility, and carrier concentration of the FTO thin films deposited by spray pyrolysis at different thicknesses
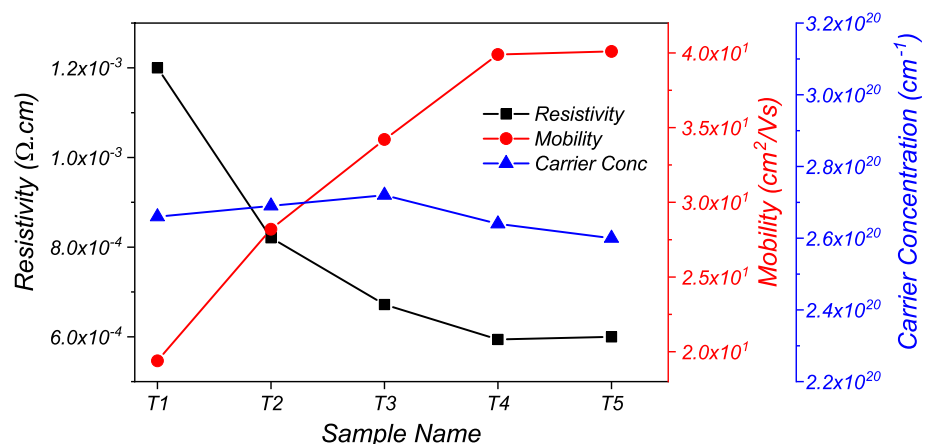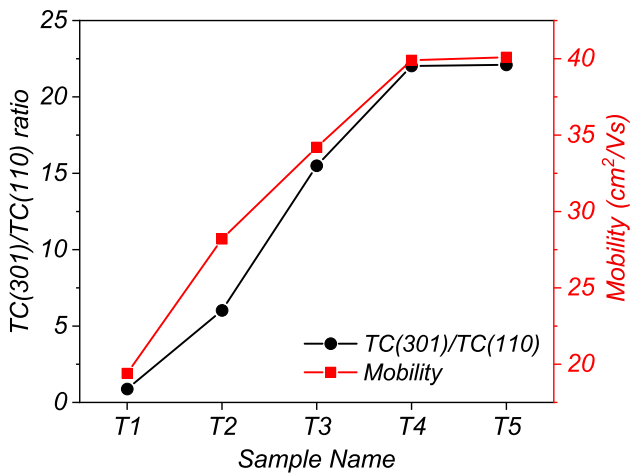
**Fig. 6** The variation of the *TC(301)/TC(110)* ratio and mobility of the prepared FTO thin films

(average transmittance of 87.33% in the 400–900 nm range) which is expectedly decreased with increasing thickness (Table 3).

The direct bandgap (E_g) of the deposited FTO thin films was estimated using the Tauc relation:

$$\alpha h\upsilon = A\left(h\upsilon - E_g\right)^n, \tag{3}$$

where $h\upsilon$ is the photon energy, A is an energy-independent constant, and n is 1/2 for direct allowed transition. The absorption coefficient (α) was calculated using transmittance (T) and reflectance (R) experimental data and the following equation:

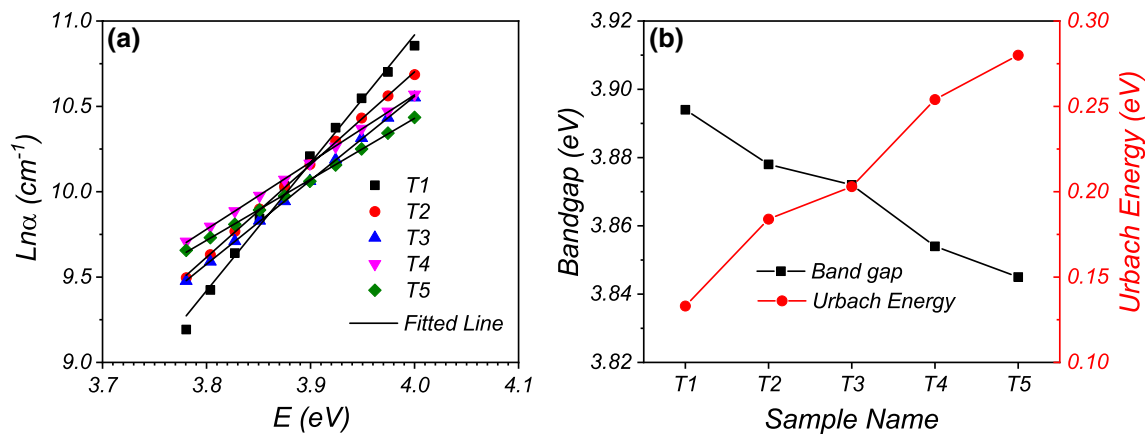$$\alpha = \frac{1}{t}\ln\left[\frac{(1-R^2)}{2T} + \sqrt{\frac{(1-R)^4}{4T^2} + R^2}\right]. \tag{4}$$
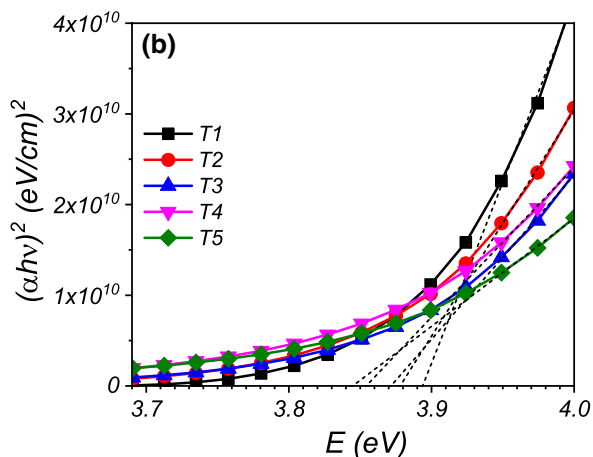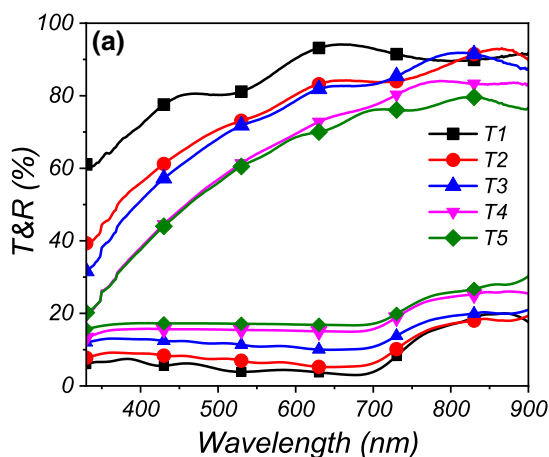
Here, t is thickness. Therefore, the bandgap can be estimated by extrapolating the linear part of $(\alpha h\upsilon)^2$ versus $h\upsilon$ to $(\alpha h\upsilon)^2 = 0$ (Fig. 7b) [32]. Moreover, the Urbach energy was estimated for the prepared FTO thin films using the following equation:

$$\alpha = \alpha_0 \exp\left(\frac{h\upsilon}{E_U}\right), \tag{5}$$

in which α_0 is a constant. To estimate the Urbach energy, the Ln(α) was plotted versus $h\upsilon$ (Fig. 8a) and the resulting slope was inverted [33]. The estimated bandgap and Urbach energy value of the spray-deposited FTO thin films with different thicknesses, which are in good agreement with the value reported in the literature [34], are listed in Table 2, and the variation is illustrated in Fig. 8b. It is clear that the band-gap value of the FTO thin film slightly decreases with increasing thickness from 3.894 for the T1 sample to 3.845 for the T5. Among the parameters which can be responsible for altering the bandgap, the increase in the crystallite size of the FTO thin films seems to be the dominant one. It is well known that the bandgap of thin films is related to the grain size through the quantum confinement effect [35]. Conversely, increasing the thickness leads to an increase in the Urbach energy (Fig. 8b) which can be related to increased disorder. The aforementioned results show a good consistency with XRD results (increase in the estimated strain values) as well as the estimated band-gap values. Based on the XRD result, the increase in thickness leads to a strain increase, which can explain the Urbach energy increase and, consequently, the reduction in the bandgap of FTO thin films [36].

To evaluate the quality of the prepared FTO thin films as a transparent conductive oxide (TCO), the Haacke's figure of merit (Φ) was calculated using the following relation:

$$\Phi = \frac{T^{10}}{R_{Sh}}, \tag{6}$$

Fig. 7 **a** The optical transmittance and reflectance spectra of the spray-deposited FTO thin films; **b** the plots of $(\alpha h\upsilon)^2$ vs. $h\upsilon$ for the estimation of the optical bandgap

Fig. 8 **a** The plot of Lnα as a function of photon energy, and **b** the variation of bandgap and Urbach energy for the spray-deposited FTO thin films

where T denotes the transmittance and R_{Sh} represents the sheet resistance of the thin film [37, 38]. The calculated results are listed in Table 3, based on which the largest value of the figure of merit belongs to the T3 sample (9.77), indicative of the best performance as a TCO from among others. Moreover, Table 4 presents a comparison between the resistivity, average transmittance, and figure of merit of the T3 sample and the best results for spray-deposited FTO thin films reported in the past.

As can be seen in Table 4, the results of the present study are considerable for spray-deposited FTO thin films. Ching-Prado et al. [11] prepared FTO thin films by spray pyrolysis technique on a glass substrate and reported resistivity of 1.15×10^{-3} Ω cm and an average transmittance of 81.2% in the visible region. Elangovan et al. [39] studied the effect of fluorine doping on the physical properties of spray-deposited FTO thin films and reached a minimum sheet resistance of 1.75 Ω sq and ~65% transmittance at 600 nm. Kumar

et al. [24] utilized nebulizer spray pyrolysis for depositing FTO thin films and investigated the effect of different solvent proportions. They achieved a minimum resistivity of 1.90×10^{-4} Ω cm and 82% transmittance for 650 nm wavelength. Purwanto et al. [38] deposited FTO thin films using flam-assisted spray and examined the influence of fluorine doping level. They reported minimum sheet resistance of 21.8 Ω sq and average transmittance of 81.9% for the wavelength range of 400–800 nm.

4 Conclusions

FTO thin films were spray-deposited on glass and, to study the effect of film thickness, the quantity of spray solution was varied from 6 to 22 ml with 4 ml steps. It was found that all the FTO thin films are polycrystalline with a tetragonal structure. Furthermore, the estimated crystallite

Table 4 The best sheet resistance, resistivity, average transmittance, and figure of merit achieved in this study compared with some of the best results for spray-deposited FTO thin films

Sheet resistance R_{Sh} (Ω sq)	Resistivity ρ ($\times 10^{-4}$ Ω cm)	Average transmittance %	Figure of merit Φ ($\times 10^{-3}$ Ω^{-1})	Technique	References
9.21	6.72	78.60 (400–900 nm)	9.77	Spray pyrolysis	This study
8.4	10	74 (at 550 nm)	5.9	Spray pyrolysis	[17]
8.43	9.86	85 (450–900 nm)	–	Spray pyrolysis	[13]
21.4	–	75.49 (400–1000 nm)	–	Spray pyrolysis	[20]
–	11.5	81.2 (visible region)	5.2	Spray pyrolysis	[11]
5.3	3.91	75 (at 550 nm)	–	Spray pyrolysis	[14]
1.75	–	~65 (at 600 nm)	11.0	Spray pyrolysis	[39]
–	6	80 (400–1100 nm)	–	Pyrosol deposition	[27]
4.96	1.90	82 (at 650 nm)	2.77	Nebulizer spray pyrolysis	[24]
21.8	–	81.9 (400–800 nm)	11	Flame-assisted spray	[38]

size and strain increased with increasing thickness. The FESEM image indicated that increasing the thickness leads to a considerable grain size enlargement. The resistivity of 5.94×10^{-4} Ω cm and average transmittance of 78.60% (400–900 nm) were achieved at the thickness of 730 nm (14 ml of spray solution). Considering the aforementioned results and the fact that the spray pyrolysis technique is cost-effective and suitable for mass production, the prepared FTO thin film can be a proper choice for TCO-based devices.

Compliance with ethical standards

References

1. H.Z. Asl, S.M. Rozati, J. Electron. Mater. **47**, 3568 (2018)
2. S.M. Rozati, S. Akesteh, Mater. Charact. **58**, 319 (2007)
3. S.V.N. Pammi, A. Chanda, N.-J. Seong, S.-G. Yoon, Chem. Phys. Lett. **490**, 234 (2010)
4. A.A. Yadav, Thin Solid Films **591**, 18 (2015)
5. R.G. Gordon, MRS Bull. **25**, 52 (2000)
6. W.-H. Baek, M. Choi, T.-S. Yoon, H.H. Lee, Y.-S. Kim, Appl. Phys. Lett. **96**, 1335061 (2010)
7. Q.-P. Tran, J.-S. Fang, T.-S. Chin, Mater. Sci. Semicond. Process. **40**, 664 (2015)
8. B.L. Zhu, F. Liu, K. Li, K. Lv, J. Wu, Z.H. Gan, J. Liu, D.W. Zeng, C.S. Xie, Ceram. Int. **43**, 10288 (2017)
9. H. Kim, R.C.Y. Auyeung, A. Piqué, Thin Solid Films **516**, 5052 (2008)
10. N. Najafi, S.M. Rozati, J. Electron. Mater. **47**, 1962 (2017)
11. E. Ching-Prado, A. Watson, H. Miranda, J. Mater. Sci. Mater. Electron. **29**, 15299 (2018)
12. M. Eslamian, Coatings **4**, 60 (2014)
13. P. Tang, C. Qiu, J. He, T. Zhang, X. Feng, X. Luo, J. Mater. Sci. Mater. Electron. **25**, 4369 (2014)
14. A.A. Yadav, E.U. Masumdar, A.V. Moholkar, K.Y. Rajpure, C.H. Bhosale, Phys B **404**, 1874 (2009)
15. A.V. Moholkar, S.M. Pawar, K.Y. Rajpure, C.H. Bhosale, Mater. Lett. **61**, 3030 (2007)
16. S.J. Ikhmayies, Int. J. Hydrog. Energy **41**, 12626 (2016)
17. N. Memarian, S.M. Rozati, E. Elamurugu, E. Fortunato, Phys. Status Solidi C **7**, 2277 (2010)
18. A. Smith, J.-M. Laurent, D.S. Smith, J.-P. Bonnet, R.R. Clemente, Thin Solid Films **266**, 20 (1995)
19. S.-T. Zhang, J.-L. Rouvière, V. Consonni, H. Roussel, L. Rapenne, E. Pernot, D. Muñoz-Rojas, A. Klein, D. Bellet, Mater. Des. **132**, 518 (2017)
20. H.S. Supriyono, Y.K. Krisnandi, J. Gunlazuardi, Procedia. Environ. Sci. **28**, 242 (2015)
21. A. Hadri, M. Taibi, M. Loghmarti, C. Nassiri, T. Slimani Tlemçani, A. Mzerd, Thin Solid Films **601**, 7 (2016)
22. A.H. Omran Alkhayatt, S.K. Hussian, Mater. Lett. **155**, 109 (2015)
23. H. Behzad, F.E. Ghodsi, J. Mater. Sci. Mater. Electron. **27**, 6096 (2016)
24. K.D.A. Kumar, S. Valanarasu, K. Jeyadheepan, H.-S. Kim, D. Vikraman, J. Mater. Sci. Mater. Electron. **29**, 3648 (2017)
25. C. Agashe, J. Hüpkes, G. Schöpe, M. Berginski, Sol. Energy Mater. Sol. Cells **93**, 1256 (2009)
26. O.S. Elsherif, G.E.A. Muftah, O. Abubaker, I.M. Dharmadasa, J. Mater. Sci. Mater. Electron. **27**, 12280 (2016)
27. J. Dutta, J. Perrin, T. Emeraud, J.-M. Laurent, A. Smith, J. Mater. Sci. **30**, 53 (1995)
28. D.H. Zhang, H.L. Ma, Appl. Phys. A **62**, 487 (1996)
29. S. Yu, L. Li, Z. Sun, H. Zheng, H. Dong, D. Xu, W. Zhang, X.D. Zhou, J. Am. Ceram. Soc. **98**, 1121 (2015)
30. R.Y. Korotkov, P. Ricou, A.J.E. Farran, Thin Solid Films **502**, 79 (2006)
31. J.T. Wang, X.L. Shi, W.W. Liu, X.H. Zhong, J.N. Wang, L. Pyrah, K.D. Sanderson, P.M. Ramsey, M. Hirata, K. Tsuri, Sci. Rep. **4**, 3679 (2014)
32. A.S. Hassanien, A.A. Akl, Superlattices Microstruct. **89**, 153 (2016)
33. C.E. Benouis, M. Benhaliliba, A. Sanchez Juarez, M.S. Aida, F. Chami, F. Yakuphanoglu, J. Alloys Compd. **490**, 62 (2010)
34. A. Abdelkrim, S. Rahmane, O. Abdelouahab, N. Abdelmalek, G. Brahim, Optik **127**, 2653 (2016)
35. H.Z. Asl, S.M. Rozati, J. Mater. Sci. Mater. Electron. **29**, 4365 (2018)
36. S. Benramache, B. Benhaoua, Superlattices Microstruct. **52**, 1062 (2012)
37. S.S. Shinde, P.S. Shinde, S.M. Pawar, A.V. Moholkar, C.H. Bhosale, K.Y. Rajpure, Solid State Sci. **10**, 1209 (2008)
38. A. Purwanto, H. Widiyandari, A. Jumari, Thin Solid Films **520**, 2092 (2012)
39. E. Elamurugu, K. Ramamurthi, J. Optoelectron. Adv. Mater. **5**, 45 (2003)